

A scalable network model for electrically tunable ferroelectric domain structure in twistrionic bilayers of two-dimensional semiconductors

V. V. Enaldiev,^{1,2,3} F. Ferreira,^{1,2} and V.I. Fal'ko^{1,2,4}

¹*University of Manchester, School of Physics and Astronomy, Oxford Road, Manchester M13 9PL, United Kingdom*

²*National Graphene Institute, University of Manchester, Booth St. E. Manchester M13 9PL, United Kingdom*

³*Kotelnikov Institute of Radio-engineering and Electronics of the RAS, Mokhovaya 11-7, Moscow 125009, Russia*

⁴*Henry Royce Institute, University of Manchester, Booth St. E. Manchester M13 9PL, United Kingdom*

Moiré structures in small-angle-twisted bilayers of two-dimensional (2D) semiconductors with a broken-symmetry interface form arrays of ferroelectric (FE) domains with periodically alternating out-of-plane polarization. Here, we propose a network theory for the tunability of such FE domain structure by applying an electric field perpendicular to the 2D crystal. Using multiscale analysis, we derive a fully parametrized string-theory-like description of the domain wall network (DWN) and show that it undergoes a qualitative change, after the arcs of partial dislocation (PD) like domain walls merge (near the network nodes) into streaks of perfect screw dislocations (PSD), which happens at a threshold displacement field dependent on the DWN period.

Two-dimensional material twistrionics, fueled by discoveries of new phenomena in twisted graphene bilayers [1–10] and trilayers [11–16], has recently expanded onto a broader range of van der Waals systems [17–23]. In general, twistrionic structures are associated with geometrical moiré patterns: a periodic variation local stacking of the two layers. In long-period moiré patterns, characteristic for small-angle-twisted bilayers, the areas of energetically preferential stacking expand into mesoscale domains [24–27], embedded into a domain wall network (DWN). In particular, by assembling a homobilayer of two inversion-asymmetric honeycomb monolayers (hBN or transition metal dichalcogenides (TMD)) with parallel orientation of their unit cells, one obtains a triangular array of domains with broken mirror and inversion symmetries [28–33] and an out-of-plane ferroelectric (FE) polarization [34–36], which direction alternates between the neighboring XM-stacking domains (metal atoms overlying chalcogens) and their MX twins (chalcogens over metal atoms) [37, 38].

The coupling between the out-of-plane FE polarization and an externally controlled displacement field, D , varies the energies of XM and MX, changing the ratio between their areas and leading to the deformation of DWN. Here, we offer a generic theory for the field-tunable FE domain structure in twistrionic TMD bilayers, fully quantified with the help of multiscale modelling approach [36, 38–40] for MX_2 -bilayers ($\text{M}=\text{Mo}, \text{W}$; $\text{X}=\text{S}, \text{Se}$). For weak fields $|D| < D_*$, the continuously deforming domain walls retain their partial dislocation character, however, above the threshold, $|D|/D_* \geq 1$, pairs of partial dislocations (PD) form streaks of perfect (full) screw dislocations (PSD, of length \mathcal{L}) near the network nodes. In Fig. 1, we illustrate how the arcs of XM/MX domain walls with a universal shape merge and split apart upon the variation of D , where the threshold field and DWN parameters scale with elastic parameters of a partial dislocation and the DWN period, ℓ , as $D_* \propto 1/\ell$.

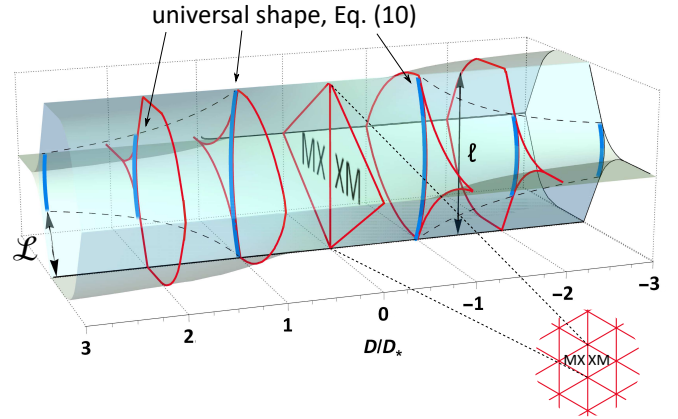


Figure 1. Triangular XM/MX DWN (inset) in twisted TMD bilayers with FE domains areas varied by an out-of-plane displacement field, D . At $D \geq D_*$, XM/MX domain walls merge into streaks of perfect screw dislocations separating - near the network nodes - domains with the same FE polarization. The remaining arcs of XM/MX domain walls have a universal shape, scaled with D_*/D ratio.

The scenario of the DWN transformation in Fig. 1 is a result of the following analysis. First, we use density functional theory (DFT) to quantify the coupling of FE polarization of an asymmetric TMD interface to an external out-of-plane displacement field, D . By taking into account the resulting coupling in the competition between the inter-layer adhesion and elastic strain in the layers, which has been used [38] and tested [27] earlier in the studies of mesoscale lattice relaxation in TMD bilayers, we derive an effective theory, formulated in terms of the DWN deformations. Finally, we find an analytical solution for such a 'string-like' theory, which has a universal form scaling with the D/D_* ratio.

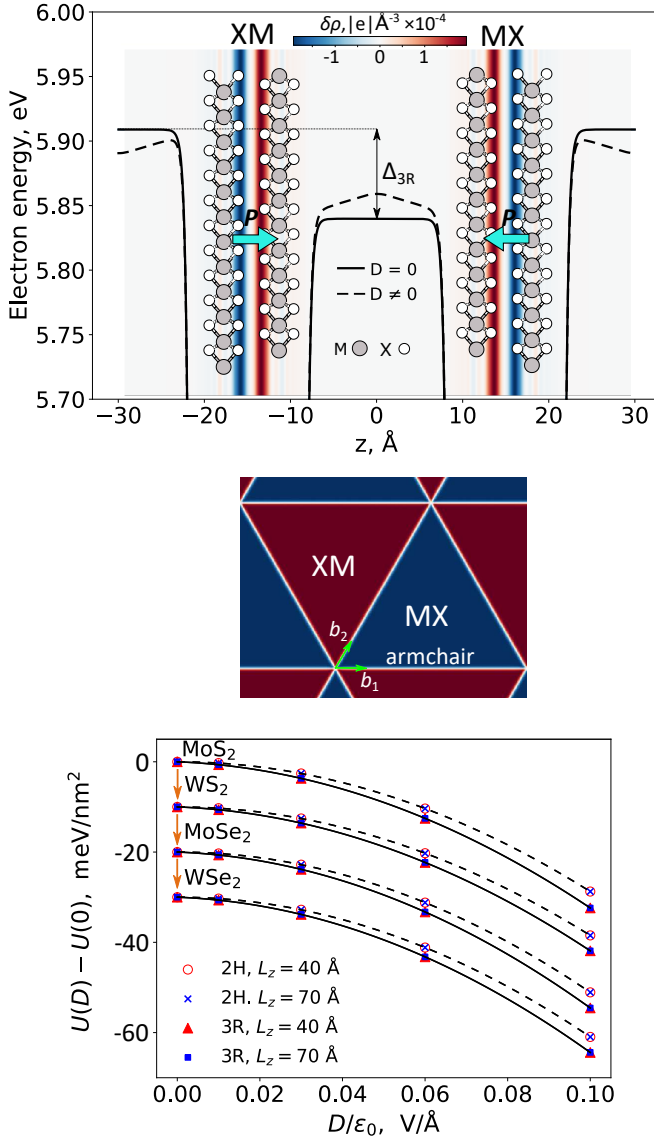


Figure 2. Top: Solid (dashed) line shows potential energy of electrons computed in DFT for a double supercell structure of TMD bilayers with 3R stacking (here, MoS₂) with and without external displacement field. A map, superimposed on the lattice structure, visualises FE charge density, $\delta\rho$ (averaged over the unit cell area). The two twin bilayers in the expanded supercell, used in the DFT modelling, represent the actual lattice structure of MX and XM domains in the reconstructed moire superlattice of a TMD bilayer, which at $D = 0$ have a triangular shape (middle panel). Bottom: DFT-computed 3R- and 2H-bilayers energy per unit cell as a function of a displacement field. Solid lines are plotted using Eq.(1) with parameters listed in Table I.

Ab initio modelling of FE bilayers in the out-of-plane electric field. Here, we use two methods to carry out DFT calculations for 3R-bilayers, with the coinciding results. In the first method, we use Quantum ESPRESSO (QE) [41, 42] to construct a supercell with a pair of mirror-reflected (MX and XM) bilayers, sepa-

rated by a large vacuum gap, as shown in Fig. 2. This choice of the structure eliminates an issue with periodic boundary condition for potential of the FE charges [36]. In the second method we construct a single 3R-bilayer and use Coulomb truncation in the out-of-plane direction [43] with QE and dipole-correction with VASP[44]. An example of the computed charge transfer, $\delta\rho$, between the layers of an individual bilayer (which integral, $\int z\delta\rho(z)dz \equiv P$, determines the areal density of the FE dipole moment) and a potential drop, Δ , across the double charge layer, is shown in Fig. 2. To mention, the computed values of P and Δ are related as $P = \epsilon_0\Delta$, in agreement with the earlier studies of 3D bulk FE materials [45].

The displacement field, accounted for by adding a triangular potential, $-D|z|/\epsilon_0$, to the input pseudopotentials, produces a shift, $\delta U \equiv U(D) - U(0)$ of the bilayer energy. The latter includes a linear term, accounting for the FE polarization, and a quadratic downward shift due to the dielectric out-of-plane polarizability of the material:

$$\delta U = -\frac{PD}{\chi\epsilon_0} - \frac{\alpha_{zz}^{3R}D^2}{2\epsilon_0\mathcal{A}}. \quad (1)$$

Here, we parametrise the $P - D$ coupling by a dimensionless parameter χ and the out-of-plane dielectric polarizability by α_{zz}^{3R} (where \mathcal{A} is the unit cell area of a TMD monolayer). The DFT-computed energies of bilayers of four different TMDs are shown in Fig. 2: in this computation, we used two different supercell periods ($L_z = 40 \text{ \AA}$ and $L_z = 70 \text{ \AA}$, which set the length of the vacuum spacer). Using Eq. (1), we find the polarizability values, which are very close to polarizability, α_{zz}^{2H} , computed for the inversion-symmetric 2H bilayer[46]. When recalculated per monolayer, these values also agree with the separately computed monolayer polarizability, α_{zz} ($\alpha_{zz} = \frac{1}{2}\alpha_{zz}^{3R} = \frac{1}{2}\alpha_{zz}^{2H}$, see in Table I). This confirms that the dielectric response of a wide band gap van der Waals materials is determined by the intra-layer polarization of the constituent atoms [47]. These values enabled us to estimate the z -axis dielectric susceptibility of bulk TMD crystals [48–50], $\epsilon_{zz} = (1 - \frac{\alpha_{zz}}{\mathcal{A}d})^{-1}$, arriving at the values in the range of $\epsilon_{zz} \sim 6 - 7.5$, listed in Table I.

Despite a substantial polarizability of monolayers, the data in Fig. 2 are described well by Eq. (1) with $\chi \approx 1$, pointing towards a decoupling of the inter-layer FE charge transfer from the intra-layer dielectric polarizability. Moreover, by comparing the DFT-computed values of the double-layer potential drop Δ to the FE coupling with the displacement field, D , in Eq. (2), we find that the linear in D energy shift in MX and XM domains (which have opposite out-of-plane FE polarization, $\pm P$, and voltage drop across the double charge layer, $\pm\Delta$) can be described very well as [51]

$$\delta U_{MX} = -\delta U_{XM} \approx -D\Delta. \quad (2)$$

Below, we will use this coupling to model tunability of the DWN by displacement field.

Table I. Dielectric and FE parameters for various TMDs. Left: polarizability (α_{zz}) (used to estimate the dielectric permittivity ϵ_{zz} of 3D-bulk TMDs), and FE coupling parameter (χ) for various 3R-TMD bilayers*). Right: FE potential drop parameters in Eq. (3).

	α_{zz}^{3R} \AA^3	α_{zz}^{2H} \AA^3	α_{zz} \AA^3	ϵ_{zz}	χ	Δ , mV	Δ_a , mV	q , nm^{-1}
MoS ₂	89.89	89.80	44.46	6.45	1.03	68	16.4	22.152
	89.93	89.85	44.48	6.48	1.02			
WS ₂	88.43	88.37	43.95	5.95	1.00	62	15	22.598
	88.43	88.37	43.94	5.95	1.00			
MoSe ₂	105.32	105.22	52.29	7.65	1.05	66	15.7	20.520
	105.31	105.25	52.24	7.67	1.07			
WSe ₂	104.37	104.33	52.03	7.39	1.04	65	15.3	20.953
	104.32	104.28	51.97	7.32	1.07			

*) For α_{zz}^{3R} , χ and ϵ_{zz} we show the values obtained with QE (top row) and - for comparison - with VASP (bottom row). For QE we used full-relativistic ultra-soft pseudo-potentials and a plane-wave cutoff energy of 70 Ry. For VASP, we used PAW full-relativistic pseudo-potentials and 60 Ry cut-off (with a $13 \times 13 \times 1$ k -point grid and a Perdew-Burke-Ernzerhof (PBE)[52] exchange-correlation functional for both QE and VASP).

Mesoscale model for lattice reconstruction is formulated in terms of the bilayer energy dependence on local stacking of the two layers and their strain [27, 38, 39], incorporated via an interlayer offset, $\mathbf{r}_0(\mathbf{r}) = \theta \hat{z} \times \mathbf{r} + \mathbf{u}^{(t)} - \mathbf{u}^{(b)}$, which varies across the superlattice, as prescribed by a small-angle, θ , misalignment between the top (t) and bottom (b) crystals and their elastic deformations, $\mathbf{u}^{(t/b)}$. Locally, stacking determines the interlayer distance, which corresponds to the minimum of the stacking-dependent adhesion energy, $\mathcal{W}(\mathbf{r}_0, d)$, quantified for the four TMDs using DFT modelling and displayed in Fig. 3. For convenience, the inter-layer distance (d) dependence of the computed $\mathcal{W}(\mathbf{r}_0, d)$ is shown as a function of $Z = d - d_0$, counted from the minimum (at $d = d_0$) of the offset-averaged adhesion energy, which coincides with $\mathcal{W}(\mathbf{r}_0 = [-a/3, 0], d)$ (one of stacking configurations shown in Fig. 3). As a result, energy density, characterizing the relaxation functional, reads:

$$\mathcal{E} = \sum_{a=t,b} \left[\frac{1}{2} \lambda \left(u_{ii}^{(a)} \right)^2 + \mu u_{ij}^{(a)} u_{ji}^{(a)} \right] + \mathcal{W}[\mathbf{r}_0(\mathbf{r}), Z] - D \Delta[\mathbf{r}_0(\mathbf{r}), Z]; \quad (3)$$

$$\mathcal{W}(\mathbf{r}_0, Z) = \kappa Z^2 + (\gamma - \gamma' Z) \sum_{n=1,2,3} \cos(\mathbf{G}_n \cdot \mathbf{r}_0).$$

Here, the first term accounts for strain, $u_{ij}^{(t/b)} = \frac{1}{2} \left(\partial_i u_j^{(t/b)} + \partial_j u_i^{(t/b)} \right)$ (λ and μ are the monolayer elastic moduli). The second term describes adhesion energy between top and bottom layers, where κ determines curvature of the adhesion energy of 3R-stacked bilayers, which characterises frequency of layer breathing mode [38], and $\mathbf{G}_{1,2,3}$ is the first star of reciprocal lattice vec-

tors of TMD monolayer, $|\mathbf{G}_{1,2,3}| = 4\pi/a\sqrt{3}$ (for details, see Refs. [27, 38, 39]). The last term is responsible for the energy shift due to the external field.

The next steps in the analysis require choosing an optimal interlayer distance between the two monolayer, which depends on the encapsulation environment of the bilayer. For a bilayer in vacuum, or encapsulated into a soft flexible matrix with a weaker adhesion to TMD than the the interlayer adhesion \mathcal{W} , we find from Eq. (3) that, locally, $Z(\mathbf{r}_0) = \frac{\gamma'}{2\kappa} \sum_n \cos(\mathbf{G}_n \cdot \mathbf{r}_0)$. For a strong substrate-TMD coupling, the monolayers would remain flat, and the optimal interlayer distance would be $Z = 0$ across the entire moiré pattern. For either of these two cases, we substitute the corresponding choice of Z in Eq. (3), and also into the local voltage drop across the double layer of charge (in the last term in Eq. (3)) corresponding to the local stacking configuration, which form has been established earlier [36]:

$$\Delta[\mathbf{r}_0, Z(\mathbf{r}_0)] = \Delta_a e^{-qZ(\mathbf{r}_0)} \sum_{n=1,2,3} \sin(\mathbf{G}_n \cdot \mathbf{r}_0).$$

For XM and MX stackings, this gives $\Delta \equiv \Delta(\mathbf{r}_0^{\text{MX}}) = -\Delta(\mathbf{r}_0^{\text{XM}})$, which values, taken from the recent *ab initio* simulations [38, 40], are listed in Table II.

Network model. While the minimization of the energy functional in (3) enables one to find all mesoscale details of the lattice adjustments of the two crystalline plane of the bilayer, it is more practical to use another method for the analysis of small-angle ($\theta \lesssim 0.5^\circ$) twisted bilayers. This is because, in the latter case, most of the areas of the moiré pattern is occupied by the homogeneous MX and XM stacking domains with a characteristic size of $\ell \gtrsim 50$ nm, whereas the deformations are concentrated inside narrow domain walls, which are only only few nanometres in width [27, 38]. Then, we define the DWN energy,

$$\mathcal{E}_\ell \equiv \int_{\text{supercell}} d^2\mathbf{r} \{ \mathcal{E} - \mathcal{W}[\mathbf{r}_0^{\text{MX}}, Z(\mathbf{r}_0^{\text{MX}})] \},$$

by subtracting the energy of a uniform MX-stacked bilayer at $D = 0$ from \mathcal{E} in Eq. (3). This reduces the problem to the analysis of \mathcal{E}_ℓ , where we can treat each domain wall as a string, characterised by energy per unit length dependent on a crystallographic orientation of the domain wall axis [38], with - as shown in Fig. 3(e) - a pronounced minimum at the armchair direction in the TMD crystal.

A finite displacement field acts as an external drive for increasing areas of domains with the preferential ferroelectric polarization. This leads to the bending of the partial dislocation (PD) domain walls, hence, increasing their energy due to their elongation and the PD axis deviation from the armchair axis. The exact form on the deformed DWN can be found by solving a 'string theory' model, expressed in terms of a deflection, $y(x)$, of PD segments from the closest armchair direction, formalised using an energy functional,

Table II. Elastic moduli, adhesion and partial dislocation energy density parameters for the studied TMD bilayers.

	γ , eV/nm ²	γ' , eV/nm ³	κ , eV/nm ⁴	μ , N/m	λ , N/m	a , nm	d_0 , nm	\bar{w} eV/nm	\tilde{w} eV/nm	u eV/nm
MoS ₂	0.189	5.634	214	70.9	83.2	0.316	0.636	0.96	0.69	2.24
WS ₂	0.212	6.327	213	72.5	52.5	0.315	0.638	1.05	0.69	2.45
MoSe ₂	0.1975	5.707	189	49.6	42.3	0.329	0.670	0.79	0.54	1.84
WSe ₂	0.1514	4.381	190	48.4	29.7	0.328	0.671	0.74	0.46	1.69

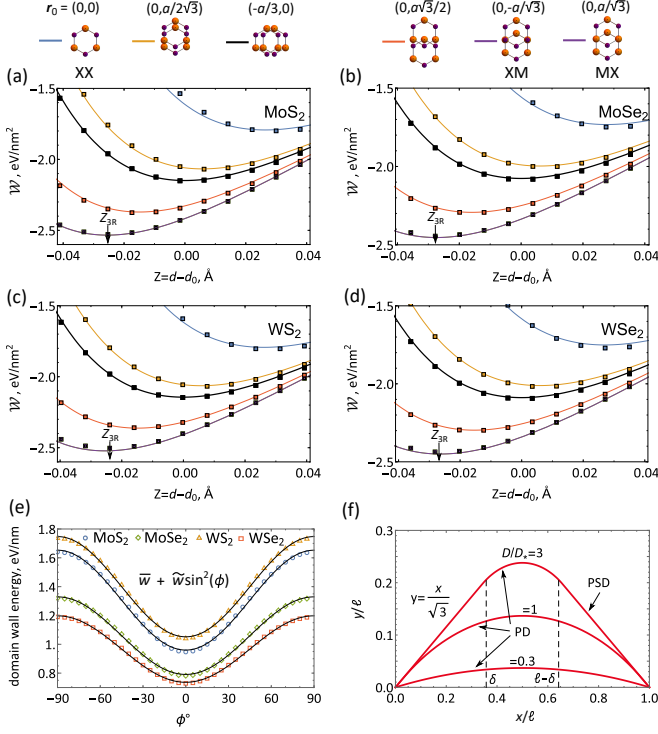


Figure 3. (a-d) TMD bilayer adhesion energies for various offsets and interlayer distances, $Z = d - d_0$, counted from the optimal distance, d_0 , of stacking configurations averaged adhesion energy. Z_{3R} labels interlayer distance used to evaluate the FE parameters in 3R (MX and XM) TMD bilayers. Details of DFT data (square dots) are described in Ref. [38]. Insets show stackings with corresponding in-plane offsets between the layers. (e) Orientation dependence of partial dislocation energy per unit length calculated in Ref. [38] and fitted with $\bar{w} + \tilde{w}\sin^2\phi$, where values of parameters are listed in Table II. $\phi = 0$ corresponds to the armchair direction. (f) Evolution of domain wall shape with displacement field, given by solution of Eq. (5) for $D < D_*$ and $D \geq D_*$.

$$\mathcal{E}_\ell[y(x), \delta] = 3 \int_\delta^{\ell-\delta} \left[\left(\bar{w} + \tilde{w} \frac{y'^2}{1+y'^2} \right) \sqrt{1+y'^2} - 2yD\Delta \right] dx + 2\sqrt{3} [u - D\Delta\delta] \delta. \quad (4)$$

Here, the first term in the integral describes the orientation-dependence of the PD energy, $\bar{w} + \tilde{w}\sin^2\phi$, and its stretching, accounted by a factor $\sqrt{1+y'^2}$ with ϕ standing for an angle between the dislocation axis and the closest armchair direction in the crystal, so that

$\sin^2\phi = y'^2/(1+y'^2)$. Two 'stiffness' parameters, \bar{w} and \tilde{w} , were determined using the data from Ref. [38], see Table II for their values for various TMDs. The second term in the integral stands for the energy gain from a bigger area of the energetically preferential FE polariza-

tion domain. The last two terms in \mathcal{E}_ℓ accounts for two PDs merging, near each DWN node, into streaks of PSDs with a length $\mathcal{L} = \delta/\sqrt{3}$ (projected onto $0 \leq x \leq \delta$ and $\delta \leq x \leq \delta - \ell$ intervals), which energetically preferable orientation is along zigzag axis in the crystal and energy per unit length is u (Table II).

Using variational principle, we obtain an equation for the the shape of each string,

$$\begin{aligned} y'' &= -\frac{2D\Delta(1+y'^2)^{\frac{5}{2}}}{\bar{w} + 2\tilde{w} + (\bar{w} - \tilde{w})y'^2}, \\ y(\delta) &= y(\ell - \delta) = \frac{\delta}{\sqrt{3}}, \end{aligned} \quad (5)$$

where δ appears as an additional variable. Note that zero values of $y(x)$ at the network nodes requires vanishing of derivative in the middle of interval, i.e. providing a symmetrical shape of the PD, with $y'(\ell/2) = 0$.

For a small D , energetically favourable domains grow due to bending of PDs, with their ends fixed at network nodes, $\delta = 0$. This elastic stretching has no threshold in D and the string form is described by [53],

$$y(x) = \int_0^x \frac{f(x')}{\sqrt{1-f^2(x')}} dx', \quad 0 \leq x \leq \ell, \quad (6)$$

where $f(x)$ is a real root of

$$f^3 - \left(\frac{\bar{w}}{\tilde{w}} + 2\right) f - 2\frac{D\Delta}{\tilde{w}} \left(x - \frac{\ell}{2}\right) = 0. \quad (7)$$

Note that $f(\ell/2) = 0$ and that $f(x) \equiv 0$ for $D = 0$.

Bending, described by Eq. (6), takes a new qualitative form after each pair of PDs near the network nodes ($x = 0$; $x = \ell$) touch each other, see Fig. 4(j). This condition corresponds to $\phi^\circ(0) = -\phi^\circ(\ell) = 30^\circ$ (i.e., $y'(0) = -y'(\ell) = 1/\sqrt{3}$), which, together with Eq. (6) determines a threshold displacement field,

$$\begin{aligned} D_* &= \epsilon_0 \frac{\mathcal{V}}{\ell}, \\ \mathcal{V} &= \frac{\left(\frac{\bar{w}}{2} + \frac{7\tilde{w}}{8}\right)}{\epsilon_0 \Delta} \Rightarrow \begin{cases} \mathcal{V}_{\text{MoS}_2} = 287 \text{ V}, \mathcal{V}_{\text{WS}_2} = 310 \text{ V}, \\ \mathcal{V}_{\text{MoSe}_2} = 236 \text{ V}, \mathcal{V}_{\text{WSe}_2} = 214 \text{ V}. \end{cases} \end{aligned} \quad (8)$$

It is important to note that pairs of touching PDs cannot annihilate, as a sum of their Burgers vectors $\mathbf{b}_1 + \mathbf{b}_2 = \mathbf{b}$ ($\mathbf{b}_1 = a(1/\sqrt{3}, 0)$, $\mathbf{b}_2 = a(1/2\sqrt{3}, 1/2)$, $\mathbf{b} = a(\sqrt{3}/2, 1/2)$) corresponds to the Burgers vector ($|\mathbf{b}| = a$) of a PSD, required to maintain an overall twist between two monolayers in the bilayer. This means that they actually form streaks of PSDs, which lengths grow with a further increase of the electric drive, as

$$\mathcal{L} = \frac{\ell}{\sqrt{3}} \left(1 - \frac{D_*}{D}\right), \quad (9)$$

The latter scaling law follows from the solution of Eq. (5) on the interval $\delta \leq x \leq \ell - \delta$ with the boundary conditions, $y'(\delta) = -y'(\ell - \delta) = 1/\sqrt{3}$, where $\delta = \sqrt{3}\mathcal{L}/2$

is a projection of \mathcal{L} onto the x -axis. Hence, above the threshold, DWN is composed of (A) PSD streaks near each network node aligned with zigzag directions in TMD, and separating the adjacent expanded energetically favourable 3R-domains and (B) PD arcs splitting up at the PSD ends, $x = \delta$ and $x = \ell - \delta$, and touching each other at the splitting points.

To find the shape of the remaining PD arcs for any $D > D_*$, we rewrite Eq. (5) in dimensionless coordinates, \tilde{x} and \tilde{y} defined by $x = \ell\tilde{x}D_*/D + \delta$, $y = \ell\tilde{y}D_*/D + \delta/\sqrt{3}$,

$$\begin{aligned} \tilde{y}'' &= -\frac{\bar{w} + \frac{7}{4}\tilde{w}}{\bar{w} + 2\tilde{w}} \frac{(1 + \tilde{y}'^2)^{\frac{5}{2}}}{1 + \frac{\bar{w} - \tilde{w}}{\bar{w} + 2\tilde{w}} \tilde{y}'^2}, \quad 0 \leq \tilde{x} \leq 1; \\ \tilde{y}'(0) &= -\tilde{y}'(1) = \frac{1}{\sqrt{3}}. \end{aligned}$$

Its solution has the same structure for any $D \geq D_*$,

$$\begin{aligned} \tilde{y}(\tilde{x}) &= \int_0^{\tilde{x}} \frac{\tilde{f}(\tilde{x}')}{\sqrt{1 - \tilde{f}^2(\tilde{x}')}} d\tilde{x}', \quad \tilde{f}(0) = \frac{1}{2}; \\ \tilde{f}^3 - \left(\frac{\bar{w}}{\tilde{w}} + 2\right) \tilde{f} - \left(\frac{\bar{w}}{\tilde{w}} + \frac{7}{4}\right) \left(\tilde{x} - \frac{1}{2}\right) &= 0, \end{aligned} \quad (10)$$

describing the universal shape of partial dislocation arcs, scaled by the ratio D_*/D , as shown in Fig. 3(f).

Finally, to validate the accuracy of the obtained analytical solution, obtained using the network model, we also performed the mesoscale lattice relaxation for a MoS₂ bilayer with a 0.1° interlayer twist (corresponding to $\ell \approx 180$ nm), by minimising the full energy functional in Eq. (3). For this, we analysed the Euler-Lagrange equations for the displacement fields $\mathbf{u}^{(t/b)}$, obtained by applying variational principle to $\mathcal{E}[\mathbf{u}^{(t/b)}]$. We solved those numerically, seeking for periodic (with the period ℓ) solutions on a sufficiently dense grid using interior point method implemented in GEKKO Optimization Suite package [54]. The computed fields were used to obtain the local values of the inter-layer offset, $\mathbf{r}_0(\mathbf{r}) = \theta\hat{z} \times \mathbf{r} + \mathbf{u}^{(t)} - \mathbf{u}^{(b)}$, which we substituted into Eqs. (3) to find the interlayer distance, Z , and to map the interlayer potential drop across the domain structure. The results for the latter quantity are shown in Fig. 4 for various values of displacement field, displaying a close agreement with the analytical solution of the network model shown by yellow lines.

To conclude, the developed effective network model gives an efficient description of the long-period domain structure in small-angle-twisted TMD bilayers with ferroelectric interface and its deformation by an out-of-plane electric field. Its analytical solution in Eqs. (6) - (10) gives a simple tool for the interpretation of experimentally measured variations of the domains' shapes, such as in the recently studied bilayers with ferroelectric properties [29–33].

Acknowledgments. We thank Andre Geim, Roman Gorbachev, Philip Kim, and David Vanderbilt for useful discussions. This study has been supported by

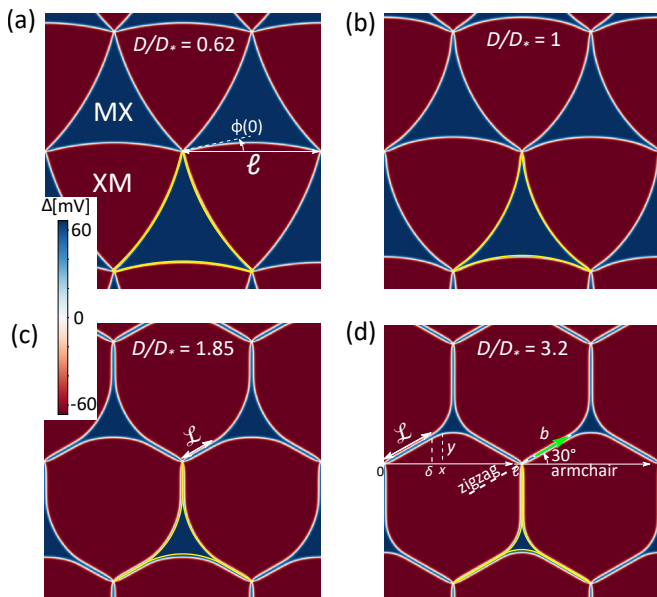


Figure 4. (a-d) Maps of the interlayer potential drop, Δ in MoS₂ bilayer with a $\theta = 0.1^\circ$ twist, computed by the minimisation of energy in Eq. (3) for various values of D below and above the threshold. These maps display the deformation of DWN from a triangular web of partial dislocations - see Figs. 1 and 2, with a $\ell \approx 180$ nm period. Yellow lines are the streaks of PSD and arcs of PD described by Eqs. (6)-(10).

the European Graphene Flagship Core3 Project, EU Quantum Flagship Project 2D-SIPC, and EPSRC grants P/W006502/1, EP/V007033/1, EP/S030719/1. The reported *ab initio* simulations were performed using EP-SRC ARCHER facility and the University of Manchester CSF.

-
- [1] Y. Cao, V. Fatemi, S. Fang, K. Watanabe, T. Taniguchi, E. Kaxiras, and P. Jarillo-Herrero, Unconventional superconductivity in magic-angle graphene superlattices, *Nature* **556**, 43 (2018).
 - [2] Y. Cao, V. Fatemi, A. Demir, S. Fang, S. L. Tomarken, J. Y. Luo, J. D. Sanchez-Yamagishi, K. Watanabe, T. Taniguchi, E. Kaxiras, and et al, Correlated insulator behaviour at half-filling in magic-angle graphene superlattices, *Nature* **556**, 80 (2018).
 - [3] M. Yankowitz, S. Chen, H. Polshyn, Y. Zhang, K. Watanabe, T. Taniguchi, D. Graf, A. F. Young, and C. R. Dean, Tuning superconductivity in twisted bilayer graphene, *Science* **363**, 1059 (2019).
 - [4] X. Lu, P. Stepanov, W. Yang, M. Xie, M. A. Aamir, I. Das, C. Urgell, K. Watanabe, T. Taniguchi, G. Zhang, *et al.*, Superconductors, orbital magnets and correlated states in magic-angle bilayer graphene, *Nature* **574**, 653 (2019).
 - [5] A. L. Sharpe, E. J. Fox, A. W. Barnard, J. Finney, K. Watanabe, T. Taniguchi, M. Kastner, and D. Goldhaber-Gordon, Emergent ferromagnetism near three-quarters filling in twisted bilayer graphene, *Science* **365**, 605 (2019).
 - [6] Y. Cao, D. Rodan-Legrain, J. M. Park, N. F. Yuan, K. Watanabe, T. Taniguchi, R. M. Fernandes, L. Fu, and P. Jarillo-Herrero, Nematicity and competing orders in superconducting magic-angle graphene, *Science* **372**, 264 (2021).
 - [7] A. Kerelsky, C. Rubio-Verdú, L. Xian, D. M. Kennes, D. Halbertal, N. Finney, L. Song, S. Turkel, L. Wang, K. Watanabe, T. Taniguchi, J. Hone, C. Dean, D. N. Basov, A. Rubio, and A. N. Pasupathy, Moiréless correlations in abca graphene, *PNAS* **118** (2021).
 - [8] S. G. Xu, A. I. Berdyugin, P. Kumaravadivel, F. Guinea, R. Krishna Kumar, D. A. Bandurin, S. V. Morozov, W. Kuang, B. Tsim, S. Liu, J. H. Edgar, I. V. Grigorieva, V. I. Fal'ko, M. Kim, and A. K. Geim, Giant oscillations in a triangular network of one-dimensional states in marginally twisted graphene, *Nature Communications* **10**, 4008 (2019).
 - [9] A. C. Gadelha, D. A. A. Ohlberg, C. Rabelo, E. G. S. Neto, T. L. Vasconcelos, J. L. Campos, J. S. Lemos, V. Ornelas, D. Miranda, R. Nadas, F. C. Santana, K. Watanabe, T. Taniguchi, B. van Troeye, M. Lamparski, V. Meunier, V.-H. Nguyen, D. Paszko, J.-C. Charlier, L. C. Campos, L. G. Cançado, G. Medeiros-Ribeiro, and A. Jorio, Localization of lattice dynamics in low-angle twisted bilayer graphene, *Nature* **590**, 405 (2021).
 - [10] N. P. Kazmierczak, M. Van Winkle, C. Ophus, K. C. Bustillo, S. Carr, H. G. Brown, J. Ciston, T. Taniguchi, K. Watanabe, and D. K. Bediako, Strain fields in twisted bilayer graphene, *Nature Materials* **20**, 956 (2021).
 - [11] H. Polshyn, J. Zhu, M. A. Kumar, Y. Zhang, F. Yang, C. L. Tschirhart, M. Serlin, K. Watanabe, T. Taniguchi, A. H. MacDonald, *et al.*, Electrical switching of magnetic order in an orbital chern insulator, *Nature* **588**, 66 (2020).
 - [12] S. Xu, M. M. Al Ezzi, N. Balakrishnan, A. Garcia-Ruiz, B. Tsim, C. Mullan, J. Barrier, N. Xin, B. A. Piot, T. Taniguchi, K. Watanabe, A. Carvalho, A. Mishchenko,

- A. K. Geim, V. I. Fal'ko, S. Adam, A. H. C. Neto, K. S. Novoselov, and Y. Shi, Tunable van der Waals singularities and correlated states in twisted monolayer–bilayer graphene, *Nature Physics* **17**, 619 (2021).
- [13] G. Chen, L. Jiang, S. Wu, B. Lyu, H. Li, B. L. Chittari, K. Watanabe, T. Taniguchi, Z. Shi, J. Jung, Y. Zhang, and F. Wang, Evidence of a gate-tunable mott insulator in a trilayer graphene moiré superlattice, *Nature Physics* **15**, 237 (2019).
- [14] C. Shen, Y. Chu, Q. Wu, N. Li, S. Wang, Y. Zhao, J. Tang, J. Liu, J. Tian, K. Watanabe, *et al.*, Correlated states in twisted double bilayer graphene, *Nature Physics* **16**, 520 (2020).
- [15] S. Chen, M. He, Y.-H. Zhang, V. Hsieh, Z. Fei, K. Watanabe, T. Taniguchi, D. H. Cobden, X. Xu, C. R. Dean, *et al.*, Electrically tunable correlated and topological states in twisted monolayer–bilayer graphene, *Nature Physics* **17**, 374 (2021).
- [16] J. M. Park, Y. Cao, K. Watanabe, T. Taniguchi, and P. Jarillo-Herrero, Tunable strongly coupled superconductivity in magic-angle twisted trilayer graphene, *Nature* **590**, 249 (2021).
- [17] J. Kunstmann, F. Mooshammer, P. Nagler, A. Chaves, F. Stein, N. Paradiso, G. Plechinger, C. Strunk, C. Schüller, G. Seifert, and *et al.*, Momentum-space indirect interlayer excitons in transition-metal dichalcogenide van der Waals heterostructures, *Nature Physics* **14**, 801 (2018).
- [18] P. Rivera, H. Yu, K. L. Seyler, N. P. Wilson, W. Yao, and X. Xu, Interlayer valley excitons in heterobilayers of transition metal dichalcogenides, *Nature Nanotechnology* **13**, 1004 (2018).
- [19] P. K. Nayak, Y. Horbatenko, S. Ahn, G. Kim, J.-U. Lee, K. Y. Ma, A.-R. Jang, H. Lim, D. Kim, S. Ryu, and *et al.*, Probing evolution of twist-angle-dependent interlayer excitons in MoSe₂/WSe₂ van der Waals heterostructures, *ACS Nano* **11**, 4041 (2017).
- [20] E. M. Alexeev, D. A. Ruiz-Tijerina, M. Danovich, M. J. Hamer, D. J. Terry, P. K. Nayak, S. Ahn, S. Pak, J. Lee, J. I. Sohn, and *et al.*, Resonantly hybridized excitons in moiré superlattices in van der Waals heterostructures, *Nature* **567**, 81 (2019).
- [21] L. J. McGilly, A. Kerelsky, N. R. Finney, K. Shapovalov, E.-M. Shih, A. Ghiotto, Y. Zeng, S. L. Moore, W. Wu, Y. Bai, K. Watanabe, T. Taniguchi, M. Stengel, L. Zhou, J. Hone, X. Zhu, D. N. Basov, C. Dean, C. E. Dreyer, and A. N. Pasupathy, Visualization of moiré superlattices, *Nature Nanotechnology* **15**, 580 (2020).
- [22] Z. Zhang, Y. Wang, K. Watanabe, T. Taniguchi, K. Ueno, E. Tutuc, and B. J. LeRoy, Flat bands in twisted bilayer transition metal dichalcogenides, *Nature Physics* **16**, 1093 (2020).
- [23] L. Wang, E.-M. Shih, A. Ghiotto, L. Xian, D. A. Rhodes, C. Tan, M. Claassen, D. M. Kennes, Y. Bai, B. Kim, K. Watanabe, T. Taniguchi, X. Zhu, J. Hone, A. Rubio, A. N. Pasupathy, and C. R. Dean, Correlated electronic phases in twisted bilayer transition metal dichalcogenides, *Nature Materials* **19**, 861 (2020).
- [24] J. S. Alden, A. W. Tsen, P. Y. Huang, R. Hovden, L. Brown, J. Park, D. A. Muller, and P. L. McEuen, Strain solitons and topological defects in bilayer graphene, *PNAS* **110**, 11256 (2013).
- [25] H. Yoo, R. Engelke, S. Carr, S. Fang, K. Zhang, P. Cazeaux, S. H. Sung, R. Hovden, A. W. Tsen, T. Taniguchi, and *et al.*, Atomic and electronic reconstruction at the van der Waals interface in twisted bilayer graphene, *Nature materials* **18**, 448 (2019).
- [26] M. R. Rosenberger, H.-J. Chuang, M. Phillips, V. P. Oleshko, K. M. McCreary, S. V. Sivaram, C. S. Hellberg, and B. T. Jonker, Twist angle-dependent atomic reconstruction and moiré patterns in transition metal dichalcogenide heterostructures, *ACS Nano* **14**, 4550 (2020).
- [27] A. Weston, Y. Zou, V. Enaldiev, A. Summerfield, N. Clark, V. Zólyomi, A. Graham, C. Yelgel, S. Magorrian, M. Zhou, J. Zultak, D. Hopkinson, A. Barinov, T. H. Bointon, A. Kretinin, N. R. Wilson, P. H. Beton, V. I. Fal'ko, S. J. Haigh, and R. Gorbachev, Atomic reconstruction in twisted bilayers of transition metal dichalcogenides, *Nature Nanotechnology* **15**, 592 (2020).
- [28] J. Sung, Y. Zhou, G. Scuri, V. Zólyomi, T. I. Andersen, H. Yoo, D. S. Wild, A. Y. Joe, R. J. Gelly, H. Heo, S. J. Magorrian, D. Bérubé, A. M. M. Valdivia, T. Taniguchi, K. Watanabe, M. D. Lukin, P. Kim, V. I. Fal'ko, and H. Park, Broken mirror symmetry in excitonic response of reconstructed domains in twisted MoSe₂/MoSe₂ bilayers, *Nature Nanotechnology* **15**, 750 (2020).
- [29] C. Woods, P. Ares, H. Nevison-Andrews, M. Holwill, R. Fabregas, F. Guinea, A. Geim, K. Novoselov, N. Walet, and L. Fumagalli, Charge-polarized interfacial superlattices in marginally twisted hexagonal boron nitride, *Nature communications* **12**, 1 (2021).
- [30] K. Yasuda, X. Wang, K. Watanabe, T. Taniguchi, and P. Jarillo-Herrero, Stacking-engineered ferroelectricity in bilayer boron nitride, *Science* **372**, 1458 (2021).
- [31] M. V. Stern, Y. Waschitz, W. Cao, I. Nevo, K. Watanabe, T. Taniguchi, E. Sela, M. Urbakh, O. Hod, and M. B. Shalom, Interfacial ferroelectricity by van der Waals sliding, *Science* **372**, 1462 (2021).
- [32] A. Weston, E. G. Castanon, V. Enaldiev, F. Ferreira, S. Bhattacharjee, S. Xu, H. Corte-Leon, Z. Wu, N. Clark, A. Summerfield, *et al.*, Interfacial ferroelectricity in marginally twisted 2D semiconductors, *arXiv:2108.06489* (2021).
- [33] X. Wang, K. Yasuda, Y. Zhang, S. Liu, K. Watanabe, T. Taniguchi, J. Hone, L. Fu, and P. Jarillo-Herrero, Interfacial ferroelectricity in rhombohedral-stacked bilayer transition metal dichalcogenides, *arXiv:2108.07659* (2021).
- [34] L. Li and M. Wu, Binary compound bilayer and multilayer with vertical polarizations: two-dimensional ferroelectrics, multiferroics, and nanogenerators, *ACS Nano* **11**, 6382 (2017).
- [35] Q. Tong, M. Chen, F. Xiao, H. Yu, and W. Yao, Interferences of electrostatic moiré potentials and bichromatic superlattices of electrons and excitons in transition metal dichalcogenides, *2D Materials* **8**, 025007 (2020).
- [36] F. Ferreira, V. V. Enaldiev, V. I. Fal'ko, and S. J. Magorrian, Weak ferroelectric charge transfer in layer-asymmetric bilayers of 2D semiconductors, *Scientific Reports* **11**, 13422 (2021).
- [37] S. Carr, D. Massatt, S. B. Torrisi, P. Cazeaux, M. Luskin, and E. Kaxiras, Relaxation and domain formation in incommensurate two-dimensional heterostructures, *Phys. Rev. B* **98**, 224102 (2018).
- [38] V. V. Enaldiev, V. Zólyomi, C. Yelgel, S. J. Magorrian, and V. I. Fal'ko, Stacking domains and dislocation networks in marginally twisted bilayers of transition metal dichalcogenides, *Phys. Rev. Lett.* **124**, 206101 (2020).

- [39] V. V. Enaldiev, F. Ferreira, S. J. Magorrian, and V. I. Fal'ko, Piezoelectric networks and ferroelectric domains in twistrionic superlattices in WS_2/MoS_2 and $\text{WSe}_2/\text{MoSe}_2$ bilayers, *2D Materials* **8**, 025030 (2021).
- [40] F. Ferreira, S. J. Magorrian, V. V. Enaldiev, D. A. Ruiz-Tijerina, and V. I. Fal'ko, Band energy landscapes in twisted homobilayers of transition metal dichalcogenides, *Applied Physics Letters* **118**, 241602 (2021).
- [41] P. Giannozzi, S. Baroni, N. Bonini, M. Calandra, R. Car, C. Cavazzoni, D. Ceresoli, G. L. Chiarotti, M. Cococcioni, I. Dabo, A. D. Corso, S. de Gironcoli, S. Fabris, G. Fratesi, R. Gebauer, U. Gerstmann, C. Gougoussis, A. Kokalj, M. Lazzeri, L. Martin-Samos, N. Marzari, F. Mauri, R. Mazzarello, S. Paolini, A. Pasquarello, L. Paulatto, C. Sbraccia, S. Scandolo, G. Sclauzero, A. P. Seitsonen, A. Smogunov, P. Umari, and R. M. Wentzcovitch, QUANTUM ESPRESSO: a modular and open-source software project for quantum simulations of materials, *Journal of Physics: Condensed Matter* **21**, 395502 (2009).
- [42] P. Giannozzi, O. Andreussi, T. Brumme, O. Bunau, M. B. Nardelli, M. Calandra, R. Car, C. Cavazzoni, D. Ceresoli, M. Cococcioni, N. Colonna, I. Carnimeo, A. D. Corso, S. de Gironcoli, P. Delugas, R. A. DiStasio, A. Ferretti, A. Floris, G. Fratesi, G. Fugallo, R. Gebauer, U. Gerstmann, F. Giustino, T. Gorni, J. Jia, M. Kawamura, H.-Y. Ko, A. Kokalj, E. Küçükbenli, M. Lazzeri, M. Marsili, N. Marzari, F. Mauri, N. L. Nguyen, H.-V. Nguyen, A. O. de-la Roza, L. Paulatto, S. Poncé, D. Rocca, R. Sabatini, B. Santra, M. Schlipf, A. P. Seitsonen, A. Smogunov, I. Timrov, T. Thonhauser, P. Umari, N. Vast, X. Wu, and S. Baroni, Advanced capabilities for materials modelling with quantum ESPRESSO, *Journal of Physics: Condensed Matter* **29**, 465901 (2017).
- [43] T. Sohier, M. Calandra, and F. Mauri, Density functional perturbation theory for gated two-dimensional heterostructures: Theoretical developments and application to flexural phonons in graphene, *Phys. Rev. B* **96**, 075448 (2017).
- [44] G. Kresse and J. Furthmüller, Efficient iterative schemes for *ab initio* total-energy calculations using a plane-wave basis set, *Physical Review B* **54**, 11169 (1996).
- [45] B. Meyer and D. Vanderbilt, Ab initio study of BaTiO_3 and PbTiO_3 surfaces in external electric fields, *Phys. Rev. B* **63**, 205426 (2001).
- [46] For monolayers and 2H-bilayers we used the Coulomb truncation in the out-of-plane direction[43].
- [47] Unlike Refs. [55, 56], which use z -averaged electric field for computation of dielectric permittivities of bilayers, we express the quadratic amendment to the total energy via out-of-plane displacement field, conserving across every cross-section of the structure. This allows us to avoid uncertainties in α_{zz}^{3R} , which may appear at averaging of the electric field in crystals with a few out-of-plane unit cells [45]. We find that the polarizability, computed for a TMD monolayer, its 2H and 3R bilayer, and thicker 2H films, linearly scales with with the number of layers. This observation contradicts some earlier DFT studies of dielectric susceptibility of TMDs [55, 56] which claimed a pronounce layer-number-dependence, but agrees with the more recent results [49] published by some of the authors of Refs [55].
- [48] S. Slizovskiy, A. Garcia-Ruiz, A. I. Berdyugin, N. Xin, T. Taniguchi, K. Watanabe, A. K. Geim, N. D. Drummond, and V. I. Fal'ko, Out-of-plane dielectric susceptibility of graphene in twistrionic and bernal bilayers, [arXiv:1912.10067](https://arxiv.org/abs/1912.10067) (2019).
- [49] T. Tian, D. Scullion, D. Hughes, L. H. Li, C.-J. Shih, J. Coleman, M. Chhowalla, and E. J. G. Santos, Electronic polarizability as the fundamental variable in the dielectric properties of two-dimensional materials, *Nano Letters* **20**, 841 (2020).
- [50] S. Slizovskiy, A. Garcia-Ruiz, A. I. Berdyugin, N. Xin, T. Taniguchi, K. Watanabe, A. K. Geim, N. D. Drummond, and V. I. Fal'ko, Out-of-plane dielectric susceptibility of graphene in twistrionic and bernal bilayers, *Nano Letters* **21**, 6678 (2021).
- [51] The expression for interaction energy of the FE polarization with displacement field naturally comes when assuming a local dielectric permittivity in a continuum medium approximation. Indeed, suppose the FE charges, with plane-averaged density $\delta\rho(z)$, are placed in the medium with local dielectric permittivity $\epsilon_{zz}(z)$. From the Poisson equation and electro-neutrality condition $\int_{-\infty}^{+\infty} \delta\rho(z)dz = 0$ $\partial_z(\epsilon_{zz}(z)\partial_z\varphi(z)) = -\delta\rho(z)/\epsilon_0$, we express the potential drop across the layer of charges as $\Delta = \int_{-\infty}^{+\infty} \partial_z\varphi(z)dz = -\int_{-\infty}^{+\infty} dz \int_{-\infty}^z dz' \delta\rho(z')/\epsilon_{zz}(z)\epsilon_0 = \int_{-\infty}^{+\infty} dz \int_z^{+\infty} dz' \delta\rho(z')/\epsilon_{zz}(z)\epsilon_0 = \int \int_{z < z'} dz dz' \delta\rho(z')/\epsilon_{zz}(z)\epsilon_0$. At the same time, interaction energy of these charges with uniform external out-of-plane displacement field (related to local electric field as $D = \epsilon_0\epsilon_{zz}(z)E(z)$) reads as $\delta U = -\int_{-\infty}^{+\infty} dz \delta\rho(z) \int_{-\infty}^z dz' D/\epsilon_{zz}(z')\epsilon_0 = -D \int_{-\infty}^{+\infty} dz' \int_{-\infty}^{z'} dz \delta\rho(z')/\epsilon_{zz}(z)\epsilon_0 = -D \int \int_{z < z'} dz dz' \delta\rho(z')/\epsilon_{zz}(z)\epsilon_0 \equiv -D\Delta$. After changing variables, $z \leftrightarrow z'$, at the last step of that calculation, we arrive at the relation in Eq. (2).
- [52] J. P. Perdew and A. Zunger, Self-interaction correction to density-functional approximations for many-electron systems, *Phys. Rev. B* **23**, 5048 (1981).
- [53] At small D (when $y'^2 \ll 1$) approximate solution of Eq. (5) is given by parabola: $y(x) = 2D\Delta(\ell - x)x/(\bar{w} + 2\tilde{w})$.
- [54] L. D. Beal, D. C. Hill, R. A. Martin, and J. D. Hedengren, Gekko optimization suite, *Processes* **6**, 106 (2018).
- [55] E. J. Santos and E. Kaxiras, Electrically driven tuning of the dielectric constant in MoS_2 layers, *ACS Nano* **7**, 10741 (2013).
- [56] A. Laturia, M. L. Van de Put, and W. G. Vandenberghe, Dielectric properties of hexagonal boron nitride and transition metal dichalcogenides: from monolayer to bulk, *npj 2D Materials and Applications* **4**, 28 (2020).